MyD88-deficient bone marrow cells accelerate onset and reduce survival in a mouse model of amyotrophic lateral sclerosis

Jihong Kang and Serge Rivest

Laboratory of Molecular Endocrinology, Centre hospitalier de l'Université Laval Research Center and Department of Anatomy and Physiology, Laval University, Québec G1V 4G2, Canada

Increasing evidence suggests that neurotoxicity of secreted superoxide dismutase 1 (SOD1) mutants is associated with amyotrophic lateral sclerosis (ALS). We show here that mutant SOD1 protein activates microglia via a myeloid differentiation factor 88 (MyD88)–dependent pathway. This inflammatory response is also associated with a marked recruitment of bone marrow–derived microglia (BMDM) in the central nervous system. We then generated chimeric SOD1^{G37R} and SOD1^{G93A} mice by transplantation of bone marrow (BM) cells from MyD88-deficient or green fluorescent protein (GFP)–expressing mice. SOD1^{G37R} mice receiving MyD88$^{-/-}$ BM cells exhibit a significantly earlier disease onset and shorter lifespan compared with mice transplanted with control GFP cells. This compelling beneficial effect of MyD88-competent BMDM is a previously unrecognized natural innate immune mechanism of neuroprotection in a mouse model of late-onset motor neuron disease.

Introduction

Amyotrophic lateral sclerosis (ALS), also known as Lou Gehrig's disease in the United States, is an adult-onset neurodegenerative disease affecting primarily motor neurons in the brain and spinal cord. The loss of motor neurons leads to the progressive atrophy of skeletal muscles and, ultimately, paralysis and death within 3–5 yr after symptom onset. About 90% of ALS cases are sporadic with no known genetic component and 10% are familial. Missense mutations in the gene encoding copper/zinc superoxide dismutase 1 (SOD1) are associated with 20% of familial ALS (Rosen et al., 1993). Transgenic mice overexpressing mutant SOD1 develop a motor neuron disease resembling ALS (Gurney et al., 1994). The inbred C57BL/6 SOD1^{G37R} mice (line 29) have a life span of ∼11–12 mo (late onset), whereas C57BL/6 SOD1^{G93A} mice exhibit a life span of ∼4–5 mo (early onset). Although these mice are two well-accepted animal models of ALS, the mechanisms leading to neurodegeneration may differ among them.

The mechanism by which SOD1 mutants cause motor neuron death is still unknown. To date, the most promising hypothesis is that the toxicity of mutant SOD1 results from the propensity of the misfolded protein mutants to aggregate rather than the aberrant copper-mediated catalysis (Johnston et al., 2000; Julien, 2001). Although SOD1 is traditionally regarded as a cytosolic protein, it is noteworthy that both wild-type (WT) and mutant SOD1 proteins can be secreted (Turner et al., 2005). A recent study proposed the selective secretion of mutant SOD1 mediated by chromogranins, which constitutes a potentially toxic pathway that can induce inflammation and neuronal death (Urushitani et al., 2006). Mutant SOD1-mediated toxicity is non–cell autonomous. The specific expression of mutant SOD1 in neurons, astrocytes, or microglia could not provoke motor neuron disease (Gong et al., 2000; Pramatarova et al., 2001; Beers et al., 2006). Over the years, increasing evidence has indicated the importance of a motor neuron milieu and the contribution of nonneuronal cells to neurodegeneration in ALS. Clement et al. (2003) demonstrated that WT nonneuronal cells delay degeneration and significantly extend survival of mutant-expressing motor neurons. More recently, it was reported that the reduced mutant SOD1 expression in microglia contributes to motor neuron protection (Boillee et al., 2006) and that WT microglia extend survival of SOD1^{G93A} mice deficient in PU.1 (Beers et al., 2006).

Microglia are the main immune cells of the central nervous system (CNS). They produce numerous inflammatory mediators, which are detected in the CNS of both mouse models and ALS patients (Nguyen et al., 2002). Up-regulation of toll-like

Correspondence to S. Rivest: serge.rivest@crchul.ulaval.ca

Abbreviations used in this paper: ALS, amyotrophic lateral sclerosis; APP, amyloid precursor protein; BM, bone marrow; BMDM, BM-derived microglia; CNS, central nervous system; FJB, fluoro-Jade B; IL, interleukin; MCP-1, monocyte chemoattractant protein 1; MyD88, myeloid differentiation factor 88; PLP1, proteolipid protein 1; SOD, superoxide dismutase; TLR2, toll-like receptor 2; WT, wild type.

The online version of this paper contains supplemental material.

The Journal of Cell Biology, Vol. 179, No. 6, December 17, 2007 1219–1230
http://www.jcb.org/cgi/doi/10.1083/jcb.200705046

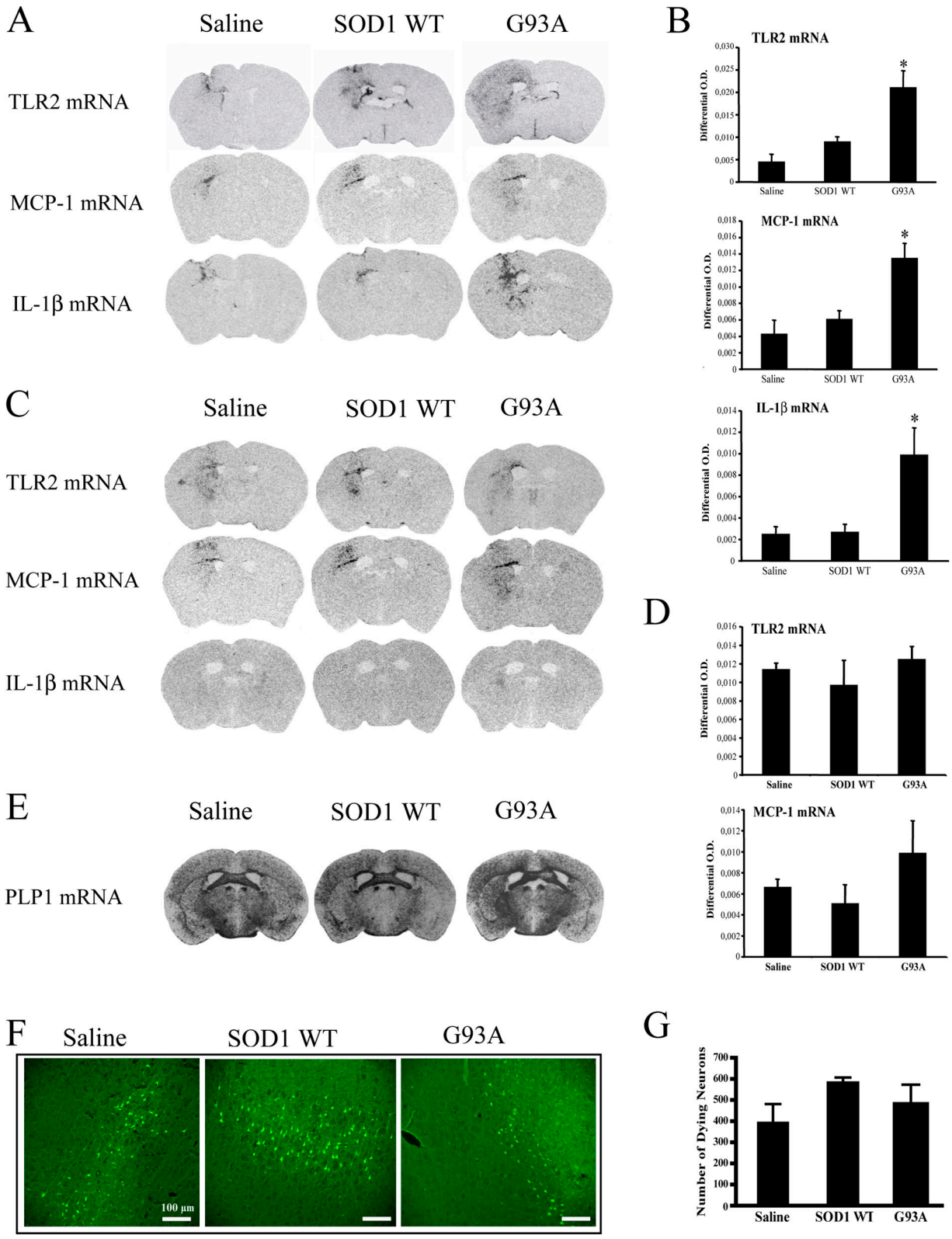

Figure 1. **Exogenous recombinant G93A form of SOD1 protein induces expression of gene encoding proinflammatory molecules.** (A) Representative photomicrographs of in situ hybridization signals showing the mRNA expression of TLR2, MCP-1, and IL-1β in the brain of adult C57BL/6J mice at 2 mo of age. Mice received a single intracerebral injection with 1 μl saline, 1 μg/μl of recombinant WT SOD1, or 1 μg/μl G93A mutant SOD1 proteins. Mice were killed 24 h after the injection. The coronal sections were taken from x-ray films. (B) Quantitative analysis of TLR2, MCP-1, and IL-1β mRNA expression. Results represent means ± the SEM of three or four mice per group. Asterisk indicates a significant difference ($P < 0.05$) from the other groups. (C) The same treatments were given to MyD88$^{-/-}$ mice. Representative in situ hybridization signals in the brain of MyD88$^{-/-}$ mice. (D) Quantitative analysis of mRNA expression in MyD88$^{-/-}$ mice. (E) Expression of the gene encoding PLP1 (a marker of oligodendrocytes) in the brains of adult C57BL/6J that received saline, recombinant WT SOD1, or G93A mutant SOD1 proteins. No sign of demyelination was found. (F) FJB staining was

receptor 2 (TLR2), a reliable index of proinflammatory signaling in microglia/macrophages, also takes place in the spinal cord of SOD1^{G37R} mice (Nguyen et al., 2004). Myeloid differentiation factor 88 (MyD88) is an adaptor protein that plays a critical role in mediating nuclear factor κB signaling and cytokine gene expression (Akira et al., 2006). The innate immune system is seriously compromised in MyD88-deficient mice (Adachi et al., 1998). Macrophages from MyD88 knockout mice did not produce interleukin (IL) 6 or TNF-α in response to lipopolysaccharide (Kawai et al., 2001). Mice deficient in MyD88 (MyD88$^{-/-}$) have impaired IL-1– and IL-18–mediated functions and defects in T-cell proliferation (Adachi et al., 1998). We used MyD88$^{-/-}$ mice to study the role of this pathway in the pathogenesis of this motor neuron disease.

We show here that extracellular mutant SOD1 induces microglial activation in vivo via a MyD88-dependent pathway. Our data from chimeric mice suggest a critical neuroprotective role of MyD88 in bone marrow–derived microglia (BMDM) in SOD1 mutant mice.

Results

Extracellular SOD1 mutant G93A induces inflammation without being neurotoxic

Adult male C57BL/6J mice at 2 mo of age were given an intracerebral injection of saline, 1 μg of recombinant human SOD1 WT, or 1 μg SOD1 mutant G93A protein. Mice were killed 3 or 24 h after the infusion. In situ hybridization was then performed across the brains of the mice using the probes for TLR2, monocyte chemoattractant protein 1 (MCP-1), TNF-α, IL-1β, IκBα, and IL-12 genes. 3 h after the treatment, the hybridization signals were comparable between different treatments (unpublished data). However, 1 d after the injection, the signal for TLR2, MCP-1, and IL-1β mRNA was higher in the brain of mice that received mutant G93A compared with WT SOD1 and saline (Fig. 1, A and B). Such an increase in gene expression was significantly prevented in MyD88-deficient mice (Fig. 1, C and D). It is interesting to note that the IL-1β mRNA signal remained undetectable in the brain of MyD88$^{-/-}$ mice. The basal levels of TLR2 are significantly higher in MyD88$^{-/-}$ compared with WT mice. These data suggest that SOD1 mutant G93A induces proinflammatory signaling via the MyD88 pathway. WT SOD1 and G93A caused a more variable expression pattern of the other immune genes measured in the present experiments. They were therefore not assessed in the brain of MyD88-deficient mice.

We next tested whether such inflammatory reaction was dependent on the potential neurotoxicity properties of the mutant protein. The expression of proteolipid protein 1 (PLP1; a marker of altered oligodendrocytes) and fluoro-Jade B (FJB; neurodegeneration) was not different in the brains of mice administered either saline, WT SOD1, or mutant SOD1 (Fig. 1, E–G). Except for the damage caused by the cannula (Fig. 1, F and G), there was no anatomical evidence of demyelination or neurodegeneration after intracerebral administration of the mutant protein. These data indicate that activation of microglia is not a consequence of the neurotoxic effects of mutant SOD1 but a direct action of the protein on these immune cells.

Infiltration of BMDM by mutant SOD1 and SOD1 mice

To determine whether this immune reaction caused infiltration of BMDM, we generated chimeric mice by transplanting GFP bone marrow (BM) cells into irradiated WT mice. 3 mo later, these mice received a single intracerebral infusion of either 1 μl saline, 1 μg/μl of recombinant human SOD1 WT, or 1 μg/μl SOD1 mutant G93A protein. 7 d after the injection, a significantly greater number of GFP cells was found in the brains of mice that received G93A protein compared with those challenged with SOD1 WT protein or saline (Fig. 2, A and B). Colocalization of green autofluorescence from GFP BM cells with Iba-1 immunostaining (Fig. 2 C, red) provided clear anatomical evidence that these GFP cells differentiated into microglia and not other cell types (Fig. 2 C). The G93A mutant is therefore able to activate microglia and provoke infiltration of BMDM.

To determine whether these events also take place in the CNS of mouse models of ALS, we generated chimeric mice by transplanting BM cells expressing GFP into irradiated SOD1^{G37R} and SOD1^{G93A} transgenic mice. Mice were killed 3, 6, and 8 mo after transplantation (SOD1^{G37R}; Fig. S1, available at http://www.jcb.org/cgi/content/full/jcb.200705046/DC1) or at the end stage (Fig. 3). A limited number of GFP cells were found in various regions of the CNS in both SOD1^{G37R} and WT groups of mice that were killed 3 and 6 mo, respectively, after being transplanted with BM cells. Numerous GFP cells were detected in the spinal cord and brain stem of SOD1^{G37R} animals at 8 mo of age (Fig. S1). At the end stage, BMDM massively infiltrated all affected regions of SOD1^{G37R} and SOD1^{G93A} chimeric mice (Fig. 3 A). All these GFP cells were immunoreactive for Iba-1 in the brain and spinal cord of SOD1^{G37R} and SOD1^{G93A} chimeric mouse models (Fig. 3 B). The data indicate that the infiltration process begins in the spinal cord and slowly progresses to more rostral degenerating regions and that all these cells differentiate into microglia in the CNS of mouse models of ALS.

MyD88$^{-/-}$ BM-derived cells significantly affect the onset and lifespan of SOD1^{G37R} mice

Based on the critical role of the MyD88 pathway in the activation of microglia by mutant SOD1 and the marked recruitment of BMDM in SOD1^{G37R} and SOD1^{G93A} chimeric mice, we attempted to explore the role of MyD88-competent BMDM. SOD1^{G37R} and SOD1^{G93A} transgenic mice were irradiated at 2 mo of age and transplanted with MyD88$^{-/-}$ or GFP BM stem cells. C57BL/6J WT mice transplanted with MyD88$^{-/-}$ or GFP BM stem cells

used as an index of neuronal cell death, which was detected in cells adjacent to the cannula's tract. Stereological quantitative analysis of the number of FJB-positive cells is shown in G. Bar, 100 μm. Results represent mean ± the SEM of four mice per group. No significant difference was observed between the groups.

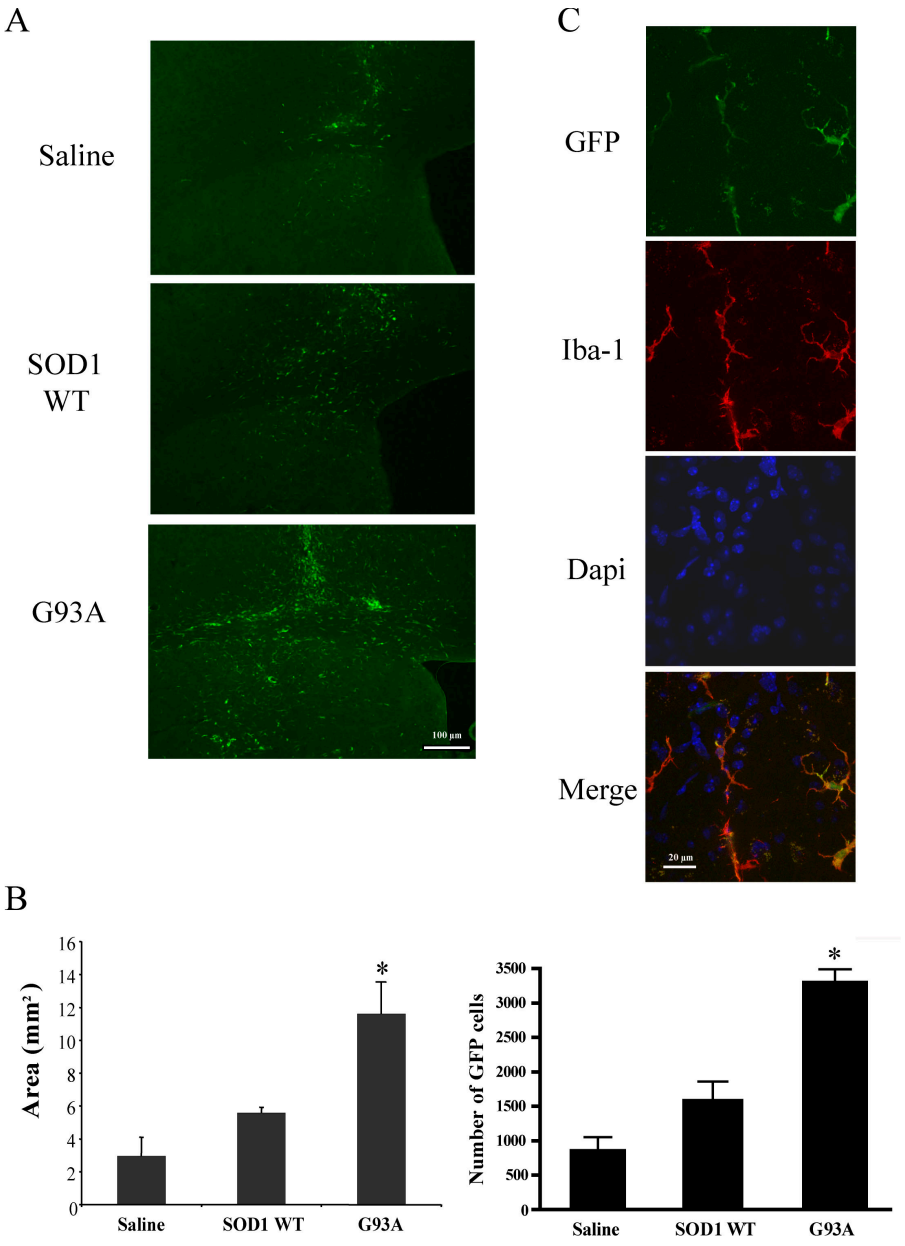

Figure 2. **Infiltration of BMDM induced by the exogenous recombinant G93A form of SOD1 protein.** GFP–C57BL/6J chimeric mice received a single intracerebral injection with 1 μl saline, 1 μg/μl recombinant WT SOD1, or 1 μg/μl G93A mutant SOD1 proteins. Mice were killed 7 d later. (A) GFP-positive cells were found in the ipsilateral side of the brain. (B) Stereological quantitative analysis of GFP-positive cells is expressed as volume in cubic millimeters and the number of cells. Results represent mean ± the SEM of four mice per group. Asterisk indicates a significant difference ($P < 0.05$) from the other groups. (C) Confocal images showing that BMDM (green) are all immunopositive for microglial cell marker Iba-1 (red; Cy3). DAPI was used to stain nuclei (blue). Bars: (A) 100 μm; (C) 20 μm.

were used as controls. We defined disease onset by the age at which a 30% decrement in motor performance was measured using a rotarod device. There was no significant difference in either symptom onset or lifespan between GFP and $SOD1^{G93A}$ chimera (GFP–$SOD1^{G93A}$) and $MyD88^{-/-}$–$SOD1^{G93A}$ groups (unpublished data). Both groups of mice became paralyzed ~1 mo after transplantation. However, $SOD1^{G37R}$ mice receiving $MyD88^{-/-}$ BM cells exhibited a significantly earlier disease onset and shorter lifespan compared with mice receiving GFP cells. The disease onset occurred at the mean age of 283 ± 2.76 d in $MyD88^{-/-}$–$SOD1^{G37R}$ mice compared with 327 ± 4.13 d in GFP–$SOD1^{G37R}$ mice (Fig. 4 A; $P < 0.001$). A remarkable difference was also found in lifespan, with a mean of 297 ± 2.4 d for $MyD88^{-/-}$–$SOD1^{G37R}$ mice and 348 ± 3.5 d for GFP–$SOD1^{G37R}$ mice (Fig. 4 B; $P < 0.001$). However, the disease duration was not significantly different between these two groups (Fig. 4 C; $P > 0.05$). Consistent with their earlier disease onset, $MyD88^{-/-}$–$SOD1^{G37R}$ mice started to lose body weight earlier than GFP–$SOD1^{G37R}$ mice (Fig. 4 D). The mean body weight of GFP–$SOD1^{G37R}$ mice was not as high as nonirradiated $SOD1^{G37R}$ mice, suggesting a potential side effect of irradiation and BM transplantation process but not on the lifespan. GFP–WT and $MyD88^{-/-}$–WT mice did not exhibit any signs of paralysis (unpublished data).

Loss of motor neurons and axons in $MyD88^{-/-}$–$SOD1^{G37R}$ chimeric mice

To compare the number of motor axons and neurons between the different groups, $MyD88^{-/-}$–$SOD1^{G37R}$ chimeric mice were killed at the end stage together with $MyD88^{-/-}$–WT and GFP–$SOD1^{G37R}$ chimeric mice. All the groups therefore had the same age but only $MyD88^{-/-}$–$SOD1^{G37R}$ animals were at the end stage.

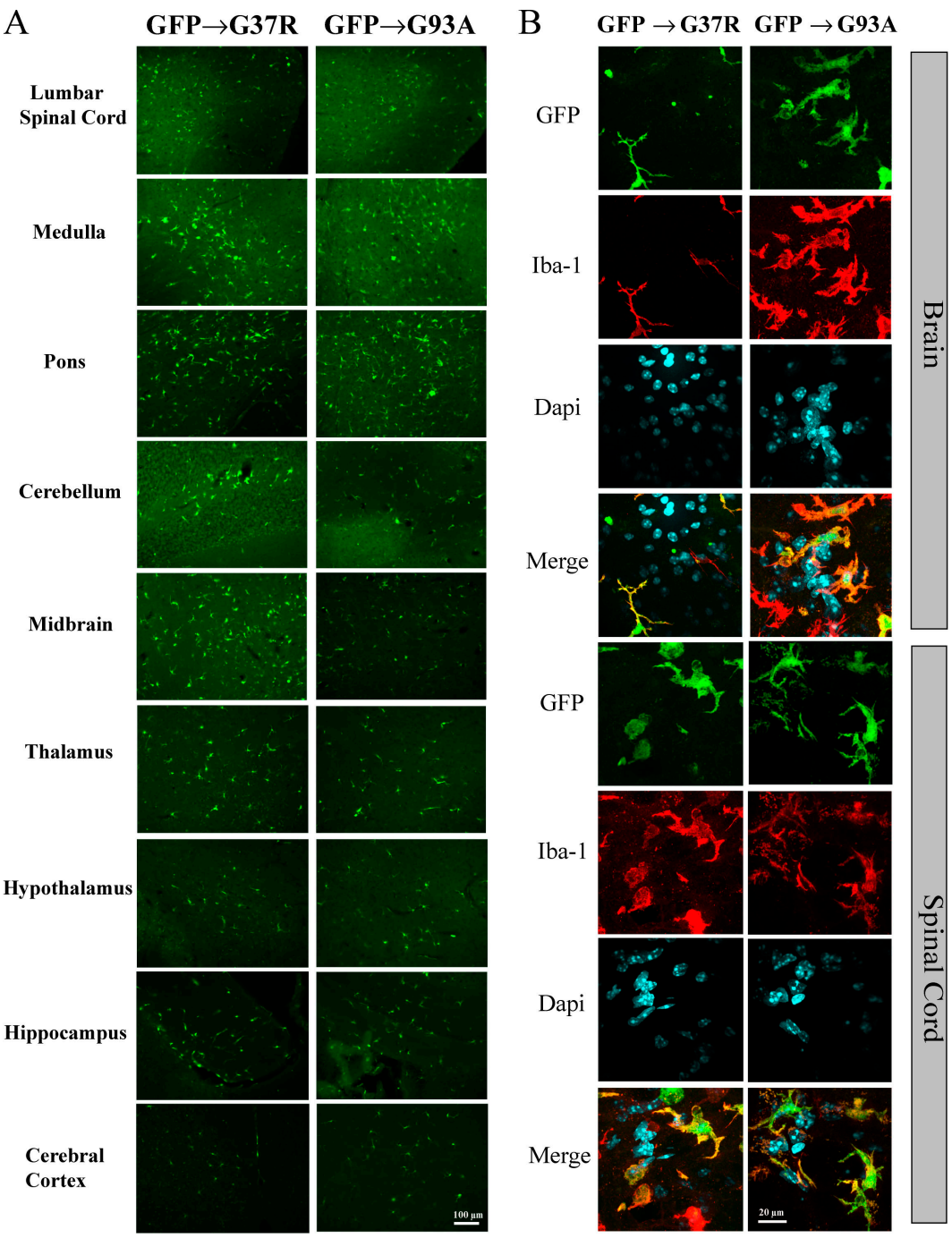

Figure 3. **Widespread distribution of BMDM in SOD1 chimeric mice.** SOD1^{G37R} and SOD1^{G93A} mice were transplanted with BM cells from GFP transgenic mice. Spinal cords and brains were taken at the end stage of the animals. (A) GFP-positive cells were detected in the lumbar spinal cord and throughout the affected regions of these two types of chimeric mice. (B) Confocal images show that BM-derived GFP-positive cells (green) in the brain and spinal cord are all microglial cells (Iba-1, red; Cy3) in both types of chimeric mice. DAPI was used to stain nuclei (blue). Bars: (A) 100 μm; (B) 20 μm.

L5 roots and lumbar spinal cords were taken from these mice and processed for the quantification of motor axons and neurons. As depicted by Fig. 5 (A and E), MyD88$^{-/-}$–SOD1^{G37R} had significantly fewer motor axons and neurons than MyD88$^{-/-}$–WT and GFP–SOD1^{G37R} chimeric mice. MyD88$^{-/-}$–SOD1^{G37R} mice had 230 ± 15 axons, whereas 787 ± 36 axons were counted in GFP–SOD1^{G37R} mice ($P < 0.05$) and 1,001 ± 21 axons in MyD88$^{-/-}$–WT ($P < 0.001$). Nissl-stained sections were used for the quantification of motor neurons in the ventral horn of lumbar spinal cords. Here again, the number of motor neurons in MyD88$^{-/-}$–SOD1^{G37R} mice (6.8 ± 0.1) was significantly lower compared with that of MyD88$^{-/-}$–WT (17.4 ± 0.5) and GFP–SOD1^{G37R} (14.7 ± 0.9) chimeric mice (Fig. 5, B and F).

It is interesting to note the strong microgliosis in the spinal cord of SOD1^{G37R}, especially in MyD88$^{-/-}$–SOD1^{G37R} chimeric mice (Fig. 5, C and D). Both the number of microglial cells and

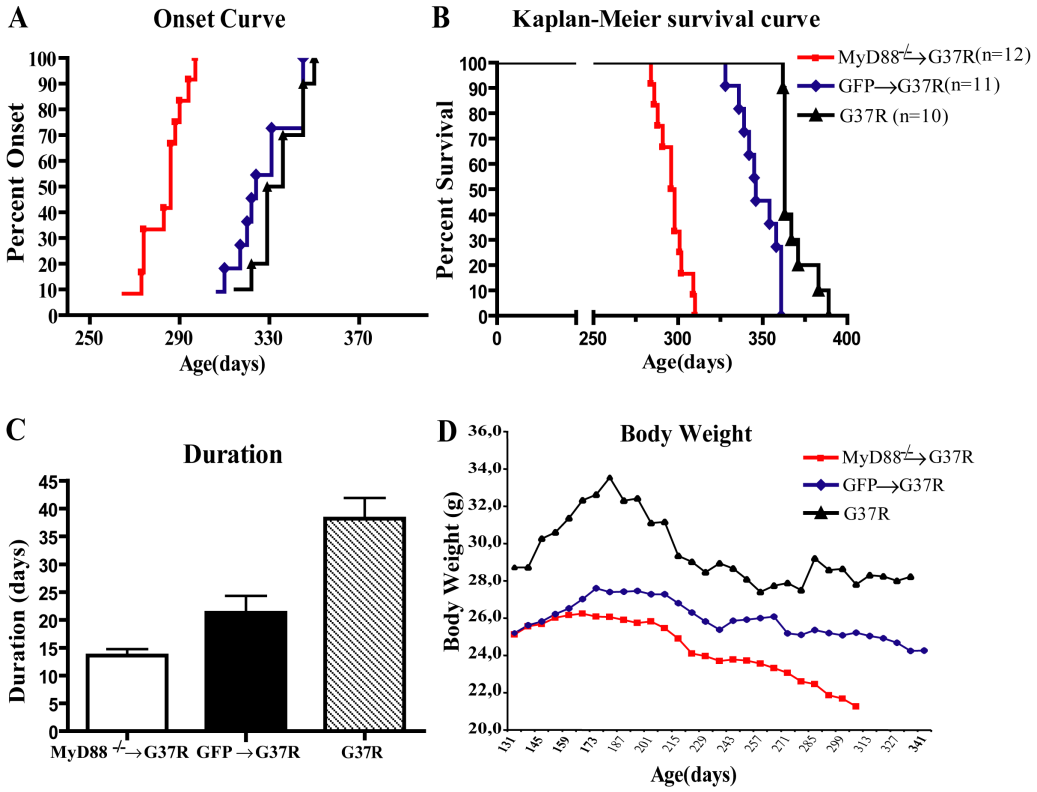

Figure 4. **Earlier disease onset and shorter lifespan of SOD1^{G37R} chimeric mice transplanted with MyD88$^{-/-}$ BM cells.** (A) The disease onset curve of MyD88$^{-/-}$–SOD1^{G37R} chimeric mice (n = 12, male), GFP–SOD1^{G37R} chimeric mice (n = 11, male), and SOD1^{G37R} mice (n = 10, male). MyD88$^{-/-}$–SOD1^{G37R} chimeric mice started the disease phenotype earlier than SOD1^{G37R} mice that received GFP BM stem cells. (B) Kaplan-Meier survival curve. MyD88$^{-/-}$ BM cells resulted in the earlier death of SOD1^{G37R} compared with SOD1^{G37R} mice transplanted with BM cells taken from GFP transgenic mice. (C) Disease duration was not significantly different between the groups. Results represent mean ± SEM of 12 mice in the MyD88$^{-/-}$–SOD1^{G37R} group, 11 mice in the GFP–SOD1^{G37R} group, and 10 mice in the SOD1^{G37R} group. (D) Weekly body weight of MyD88$^{-/-}$–SOD1^{G37R} chimeric, GFP–SOD1^{G37R} chimeric, and SOD1^{G37R} transgenic mice.

the hybridization signal for the gene encoding the innate receptor TLR2 were significantly higher in mice that were transplanted with MyD88-deficient BM cells (Fig. 5, C, D, and G). Transcriptional activation of TLR2 is a reliable marker of the innate immune response by microglia (Laflamme et al., 2001; Nguyen et al., 2002). Whether such a microgliosis contributes or is a consequence of the rapid and marked neurodegeneration in MyD88$^{-/-}$–SOD1^{G37R} mice remains an open question.

Role of MyD88 in SOD1^{G93A} and SOD1^{G37R} mice

Because MyD88 plays a critical role in the BMDM of SOD1^{G37R} animals and MyD88$^{-/-}$–SOD1^{G37R} chimeric mice exhibited a robust innate immune reaction in the spinal cord (Fig. 5, C and D), we created SOD1^{G93A} and SOD1^{G37R} mice in the context of a MyD88 gene knockout. However, we were not able to generate a single SOD1^{G93A};MyD88$^{-/-}$ mouse after >1 yr of crossbreeding. It is possible that MyD88 is critical for the development and survival of these mice because of the high copy number of mutant SOD1 in the SOD1^{G93A} line, which is a rapid and severe mouse model of motor neuron degeneration. In contrast, we were able to generate SOD1^{G37R};MyD88$^{-/-}$ mice, but no significant difference was detected in the disease onset, duration, or survival between G37R$^{+/-}$;MyD88$^{-/-}$ and G37R$^{+/-}$;MyD88$^{+/+}$ groups (Fig. 6, A–C). However, the body weights of G37R$^{+/-}$;MyD88$^{-/-}$ mice were much lower than the other groups of mice (Fig. 6 D).

Characteristics of the spinal cord from the crossed mice

Crossed mice were killed at 8 mo (presymptomatic stage), 11 mo (symptomatic stage), and the end stage. To examine whether the context of MyD88 deficiency affects motor neurons, Nissl staining was performed and motor neurons were counted in the ventral horn of lumbar spinal cords. No significant difference was found between G37R$^{+/-}$;MyD88$^{+/+}$ and G37R$^{+/-}$;MyD88$^{-/-}$ at the presymptomatic stage. Although not statistically significant, G37R$^{+/-}$;MyD88$^{-/-}$ mice appeared to have fewer motor neurons than G37R$^{+/-}$;MyD88$^{+/+}$ mice at 11 mo. However, G37R$^{+/-}$;MyD88$^{-/-}$ mice had significantly fewer motor neurons in the lumbar spinal cord compared with G37R$^{+/-}$;MyD88$^{+/+}$ mice at the end stage of the disease ($P < 0.05$; Fig. 7 A). Immunohistochemistry with the use of microglial cell marker anti–rabbit Iba-1 did not reveal any major differences in the number of microglia between these two groups at the presymptomatic stage, symptomatic stage, or end stage (Fig. 7 B). TLR2 mRNA expression was found to be similar at the presymptomatic and symptomatic stages between G37R$^{+/-}$;MyD88$^{-/-}$ and

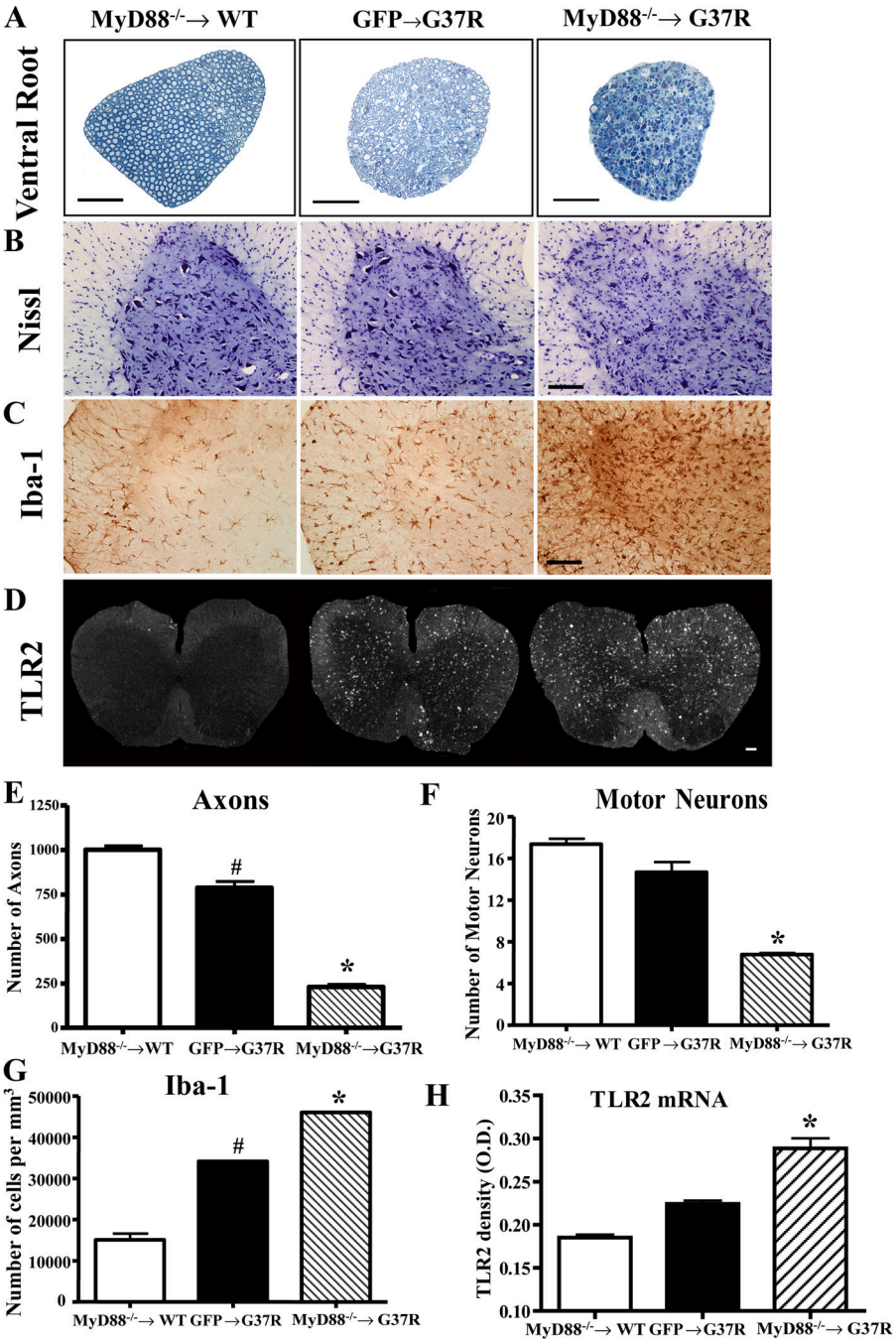

Figure 5. **Motor neuron degeneration and microgliosis in MyD88$^{-/-}$–SOD1^{G37R} chimeric mice.** MyD88$^{-/-}$–SOD1^{G37R} chimeric mice were killed at the end stage together with the same age MyD88$^{-/-}$–WT and GFP–SOD1^{G37R} chimeric mice. Tissue samples from the three groups of mice were analyzed. (A) Images of transverse sections of L5 ventral root. Massive degeneration was observed in the L5 ventral root of MyD88$^{-/-}$–SOD1^{G37R} chimeric mice. The counting of motor axons is shown in E. (B) Nissl staining of transverse sections of lumbar spinal cord. Motor neurons were counted and statistical analysis is shown in F. (C) Immunohistochemical staining of lumbar spinal cord with the use of microglial cell marker anti–rabbit Iba-1 followed by incubation with biotinylated secondary antibody. The numbers of microglial cells were estimated, expressed as number of cells per cubic millimeter, and shown in G. (D) In situ hybridization using antisense probe for TLR2 gene. Dark-field photomicrographs showing increased TLR2 mRNA hybridization signals in emulsion-dipped lumbar spinal sections from MyD88$^{-/-}$–SOD1^{G37R} chimeric mice compared with the control mice. (H) Quantitative analysis of TLR2 mRNA expression. Results represent means ± the SEM of three mice per group. Asterisk indicates a significant difference ($P < 0.05$) from the other groups. Number sign indicates a significant difference ($P < 0.05$) from MyD88$^{-/-}$–WT group. Bars, 100 μm.

G37R$^{+/-}$;MyD88$^{+/+}$ groups, but the signal was much higher in the lumbar spinal cord of G37R$^{+/-}$;MyD88$^{-/-}$ compared with G37R$^{+/-}$;MyD88$^{+/+}$ at the end stage of the disease ($P < 0.05$; Fig. 7 C).

Discussion

Although ALS was first described in 1869, the mechanisms involved in the pathogenesis of this neurodegenerative disease still remain largely unknown. Several mechanisms that are not mutually exclusive have been proposed. These include oxidative stress, glutamate-induced excitotoxicity, cytoskeletal abnormalities, protein aggregation, mitochondrial dysfunction, and, more recently, inflammation. The role of inflammation and microglia in ALS and other CNS diseases is currently a matter of great debate and controversy. Although numerous cytokines are upregulated in microglia of mice expressing mutant SOD1 transgenes, deletion in the gene encoding IL-1β and TNF does not change the outcomes of the diseases (Nguyen et al., 2001; Gowing et al., 2006). However, SOD1^{G37R} mice that had MyD88-competent BMDM developed the disease later, survived longer, and had less neurodegeneration than those that were transplanted with MyD88-deficient BM cells. These data suggest a novel neuroprotective role of competent BMDM in a mouse model of ALS.

The discovery that ∼20% of familial ALS cases are caused by mutations in SOD1 has enabled the development of animal

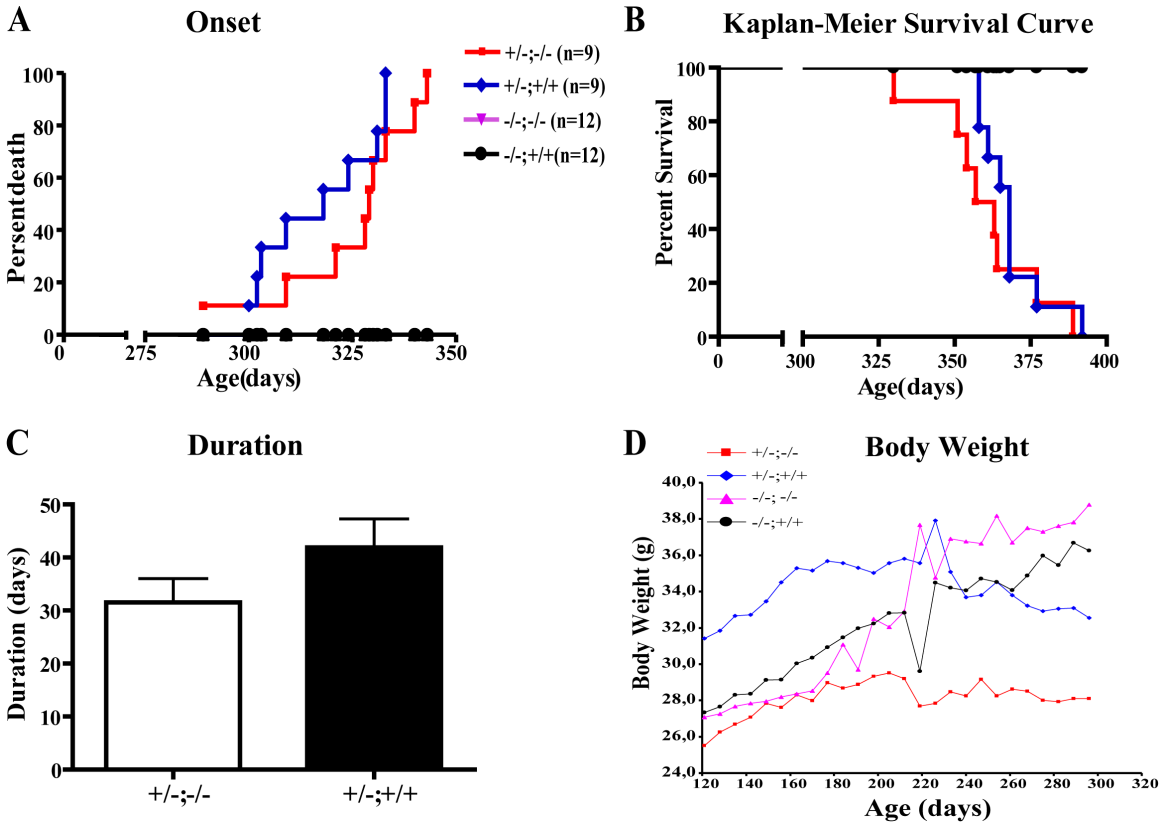

Figure 6. **The absence of MyD88 does not affect SOD1^{G37R} mice.** SOD1^{G37R} mice were bred with MyD88$^{-/-}$ (G37R$^{+/-}$;MyD88$^{-/-}$). Four groups of crossed mice with the following genotypes were compared: G37R$^{+/-}$;MyD88$^{-/-}$ (n = 9; five females and four males), G37R$^{+/-}$;MyD88$^{+/+}$ (n = 9; four females and five males), G37R$^{-/-}$;MyD88$^{-/-}$ (n = 12; five females and seven males), and G37R$^{-/-}$;MyD88$^{+/+}$ (n = 12; six females and six males). (A) The disease onset curve. (B) Kaplan-Meier survival curve. (C) Disease duration histogram. Results represent mean ± the SEM of nine mice per group. (D) Growth curve. No significant difference was observed in disease onset, survival, or disease duration between G37R$^{+/-}$;MyD88$^{-/-}$ and G37R$^{+/-}$;MyD88$^{+/+}$ groups.

and cell culture models and led to much of our current understanding of the neurodegenerative mechanisms in ALS. SOD1 is a ubiquitously expressed protein, which protects cells from damage by free radicals. ALS often starts focally. It is still unclear how the toxicity of mutant SOD1 is propagated from one localized group of cells to another. Based on the recent evidence that extracellular mutant SOD1 proteins could be selectively secreted and trigger microgliosis and neuronal death in cultured cells (Urushitani et al., 2006), we injected WT SOD1 and mutant proteins into the mouse CNS. G93A mutant protein was used in our experiments because it was the only SOD1 mutant protein available to us. In agreement with this study, our data demonstrate that mutant SOD1 stimulates inflammation and recruitment of BMDM. WT SOD1 protein was used as a control to ascertain that these effects were specific to the mutant protein and not to potential traces of endotoxin. The inflammatory response caused by G93A is largely dependent on MyD88 signaling but it is still not known whether this protein binds to specific immune receptors in microglia. However, G93A is able to stimulate TNF production from the microglial cell line (Urushitani et al., 2006) and an acute intracerebral infusion of this protein is not neurotoxic. We therefore suggest that the inflammatory properties of mutant SOD1 are directly mediated by the MyD88 pathway in microglia and not via other products released by dying cells.

Previous studies have shown that in chimeric SOD1^{G93A} mice, BM-derived cells differentiate into microglia in the spinal cord and brain. In addition, it has been suggested that the number of GFP-positive cells in the spinal cord is associated with disease progression (Corti et al., 2004; Solomon et al., 2006). In this paper, we generated chimeric SOD1^{G37R} and SOD1^{G93A} mice and confirmed the extensive distribution of GFP-positive cells throughout the brain and spinal cord in both mouse models of ALS. In accordance with the previous studies, we observed few GFP-positive cells in the CNS before the disease onset (Fig. S1), but the number of GFP cells greatly increased during disease progression (Table S1, available at http://www.jcb.org/cgi/content/full/jcb.200705046/DC1). More importantly, transplantation of BM from GFP- expressing mice does not affect disease progression of either SOD1^{G93A} or SOD1^{G37R} mice when compared with their respective nonirradiated SOD1 groups. In contrast, transplantation of MyD88-deficient BM cells dramatically changed the disease onset and progression only in mice that express human mutant G37R.

The rationale to investigate the role of this adaptor protein was based on our initial observation that the MyD88 pathway mediates microglial activation and infiltration induced by mutant SOD1. The results from the chimeric mice suggest that BMDM acts as a natural defense mechanism against secreted mutant SOD1.

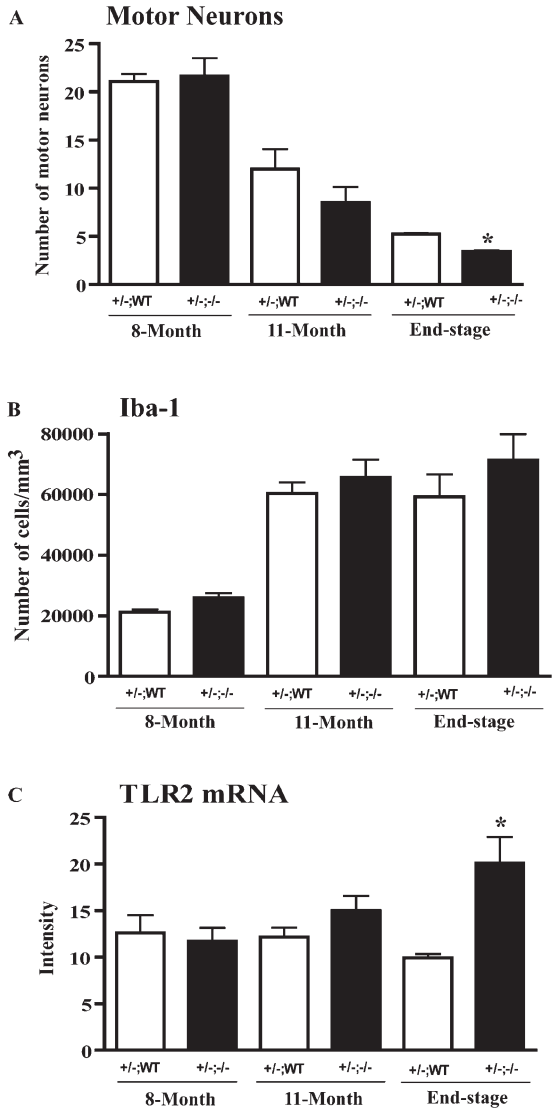

Figure 7. **Number of motor neurons and microglia in the spinal cord of SOD1^{G37R} mice in a MyD88 knockout context.** Crossed mice were killed at 8 mo (presymptomatic stage), 11 mo (symptomatic stage), and the end stage. Results represent mean ± the SEM of four mice per group. (A) Motor neurons were counted in the lumbar spinal cord. Note a significant difference between the groups of G37R$^{+/-}$;MyD88$^{+/+}$ and G37R$^{+/-}$;MyD88$^{-/-}$ at the end stage ($P < 0.05$). (B) Immunohistochemical staining of lumbar spinal cord with the use of microglial cell marker anti–rabbit Iba-1 followed by the incubation with biotinylated secondary antibody. The numbers of microglial cells were estimated and expressed as the number of cells per cubic millimeter. No significant difference was found between the groups of G37R$^{+/-}$;MyD88$^{+/+}$ and G37R$^{+/-}$;MyD88$^{-/-}$ at the presymptomatic, symptomatic, or end stage ($P > 0.05$). (C) In situ hybridization was performed using antisense probe for TLR2 gene. Quantitative analysis of TLR2 mRNA expression showed a significant difference between the groups G37R$^{+/-}$;MyD88$^{+/+}$ and G37R$^{+/-}$;MyD88$^{-/-}$ at the end-stage ($P < 0.05$). These data indicate that microglial cells were more activated in G37R$^{+/-}$;MyD88$^{-/-}$ mice.

Indeed, MyD88$^{-/-}$ BM transplantation led to the earlier disease onset and shorter lifespan of SOD1^{G37R} mice compared with mice that received GFP cells. GFP–SOD1^{G37R} and nonirradiated SOD1^{G37R} mice were used as controls to exclude the possibility that these effects were attributable to irradiation. Histological analysis revealed a significant motor neuron and axon loss in MyD88$^{-/-}$– SOD1^{G37R} mice compared with the GFP–SOD1^{G37R} and MyD88$^{-/-}$–WT mice at the same age, which explains the intriguing earlier disease onset and death of MyD88$^{-/-}$– SOD1^{G37R} mice. We also found a more robust innate immune reaction in the spinal cord of these mice.

It has been shown that WT nonneuronal cells delayed disease onset by a mean of 1.2 mo for SOD1^{G37R} chimeras and extended their survival by 1.1 mo (Clement et al., 2003). A recent study demonstrated that substitution of WT microglia for SOD1^{G93A}-expressing microglia prolonged the survival and disease duration of SOD1^{G93A} mice but had no effect on the onset (Beers et al., 2006). However, reduced levels of mutant SOD1 in microglia did not change onset and the early disease phase but clearly slowed later paralysis (Beers et al., 2006; Boillee et al., 2006). These data do not necessarily contradict the experiments using MyD88-deficient mice. Indeed, the disease progression may be influenced by the levels of extracellular mutant SOD1 that resident microglia contribute to this extracellular pool. This may be an explanation for the neuroprotective properties of SOD1-deficient microglia and such effects may not be associated with the immune functions of these cells.

We have previously reported the existence of different populations of microglia that may have somewhat opposite roles. The double-edged sword of these cells that has been intensively reviewed in the past few years may also depend on the origin of microglia in the adult CNS. BMDM are very efficient in restricting amyloid deposits in a mouse model of Alzheimer's disease, whereas their resident counterparts seem unable to phagocyte this toxic protein (Simard et al., 2006). The results from this paper support this concept and imply that impairment of such natural function of BMDM accelerates the neurodegenerative properties of secreted mutant SOD1. It is interesting to note that transplantation of MyD88-deficient BM cells did not change onset or survival of mice expressing human SOD1^{G93A}. These mice reach paralytic endstage ~2 mo after BM transplantation. The hematopoietic system takes 7–9 wk to be fully restored after lethal irradiation and the percentage of GFP- or MyD88-deficient cells is low during the first 4 wk of the chimera. This may explain why these cells are unable to modulate the disease progression in such an early onset model of neurodegeneration. This is not the case in mice expressing SOD1^{G37R} because restoration of BMDM is completed in these animals several months before the first symptomatic signs. The early onset may therefore explain why MyD88$^{-/-}$ BM cells failed to change the mean life expectancy of SOD1^{G93A}.

Because of the potent beneficial role of WT BMDM in SOD1^{G37R} mice, the lack of significant difference in the disease onset and lifespan between G37R$^{+/-}$;MyD88$^{-/-}$ and G37R$^{+/-}$;MyD88$^{+/+}$ groups of mice may seem surprising. However, histological analysis revealed that microglial cells seem to be much more activated in G37R$^{+/-}$;MyD88$^{-/-}$ compared with G37R$^{+/-}$;MyD88$^{+/+}$ mice at the end stage of the disease (Fig. 7 C). In addition, at the end stage, G37R$^{+/-}$;MyD88$^{-/-}$ mice lost significantly more motor neurons than G37R$^{+/-}$;MyD88$^{+/+}$ mice (Fig. 7 A), which suggests that the context of MyD88 deficiency does affect these SOD1^{G37R} mice. Neuroprotection is not always associated with a significant extension of survival in mouse

models of ALS. A recent study has shown that sodium valproate, the histone deacetylase inhibitor, exerts neuroprotective effects both in vitro and in vivo but it does not improve the survival of $SOD1^{G86R}$ mice (Rouaux, et al., 2007).

It is also important to mention that $G37R^{+/-}$;$MyD88^{-/-}$ mice were much smaller than their littermates based on weekly body weight. In addition, the numbers of pups per carriage was lower in $G37R^{+/-}$;$MyD88^{-/-}$ mice, with a mean of 4.5 compared with 7 pups from SOD1, 6 from $MyD88^{-/-}$, and 8 from WT mice. Moreover, we were not able to generate a single $G93A^{+/-}$;$MyD88^{-/-}$ mouse after >1 yr of crossbreeding between $SOD1^{G93A}$ and MyD88-deficient mice. We have not been able to generate homozygote $MyD88^{-/-}$ mice in using another mouse model of brain disease. Indeed, for >2 yr, we have attempted to breed amyloid precursor protein (APP)/presenelin 1 transgenic mice with our $MyD88^{-/-}$ colony and we have obtained only APP;$MyD88^{+/-}$ but not a single APP;$MyD88^{-/-}$ mouse. This indicates that these MyD88 homozygotes are not viable in the presence of highly toxic proteins, such as G93A and APP/presenelin 1. Compared with $SOD1^{G93A}$, the lower level of $SOD1^{G37R}$ may also explain why we were able to generate $G37R^{+/-}$;$MyD88^{-/-}$ mice.

Although unexpected, it is not surprising that the blockage of the MyD88-dependent intracellular signaling pathway in SOD1 mice does not have a marked influence on the survival. Indeed, previous studies have shown that exposure of $MyD88^{-/-}$ macrophages with lipopolysaccharide results in the delayed activation of nuclear factor κB and MAPKs, which suggests the existence of a MyD88-independent signaling pathway (Kawai et al., 2001). The paradoxical results from chimeric mice (where MyD88-deficient BMDM reduced survival) and crossed mice (where absence of MyD88 did not affect disease course) are best explained by putative compensatory mechanisms activated by developmental absence of MyD88. In fact, the strategies are very different. $G37R^{+/-}$;$MyD88^{-/-}$ mice may bear the compensation throughout their life, otherwise they will not be viable. This is obviously not the case in both models of transgenic SOD1 mice transplanted with BM-deficient cells because the MyD88 gene is present during all the developmental stages and is deleted only in BM stem cells at the age of 2 mo.

In summary, our data demonstrate a critical effect of MyD88 within BMDM in a mouse model of ALS disease, which suggests a novel neuroprotective role of BMDM and supports the protective functions of microglia at the early stage of ALS disease. With further studies, we hope to find a novel approach to optimize the neuroprotective role of BMDM in ALS disease.

Materials and methods

Animals

Adult male C57BL/6J mice were purchased from the Jackson Laboratory at 2 mo of age. Hemizygous transgenic mice expressing GFP under the control of the chicken β-actin promoter and cytomegalovirus enhancer were initially also obtained from the Jackson Laboratory. A colony was then established and maintained in a C57BL/6J background. Transgenic mice carrying G37R (line 29) and those harboring the G93A mutant of human SOD1 (B6SJL-TgN[SOD1-G93A]1Gur) were obtained from J.P. Julien (Laval University, Québec, Canada). $MyD88^{-/-}$ mice (in C57BL/6 background) were provided by S. Akira (Osaka University, Osaka, Japan). $SOD1^{G93A}$ and $SOD1^{G37R}$ mice were crossed with $MyD88^{-/-}$ mice to generate $G93A^{+/-}$;$MyD88^{-/-}$ and $G37R^{+/-}$;$MyD88^{-/-}$ mice by breeding $G93A^{+/-}$ and $G37R^{+/-}$ with $MyD88^{-/-}$ mice, yielding offspring that were heterozygous for the MyD88 gene. The heterozygous offspring were intercrossed to obtain breeding pairs of the following genotypes: $G37R^{+/-}$;$MyD88^{-/-}$, $G37R^{-/-}$;$MyD88^{-/-}$, $G37R^{+/-}$;$MyD88^{+/+}$, and $G37R^{-/-}$;$MyD88^{+/+}$. With the breeding procedure, we were not able to generate $G93A^{+/-}$ in a context of MyD88 knockout (see Discussion). Animals were acclimated to standard laboratory conditions (14-h light and 10-h dark cycle; lights on at 06:00 and off at 20:00) with free access to rodent feed and water. All animal protocols were approved by the Laval University Animal Welfare Committee in accordance with the Canadian Council on Animal Care guidelines.

BM transplantation

Irradiation and BM transplantation were performed as described previously (Simard and Rivest, 2004; Simard et al., 2006). In brief, mice at 2 mo of age were exposed to 10 gray total-body irradiation using a cobalt-60 source (Theratron-780; MDS Analytical Technologies). A few hours later, the animals were injected via a tail vein with $\sim 14 \times 10^6$ BM cells freshly collected and purified from donor mice. GFP or $MyD88^{-/-}$ mice at 3–5 mo of age were used as cell donors. Irradiated mice transplanted with BM cells were housed in autoclaved cages and treated with antibiotics (0.2 mg trimethorpine and 1 mg sulfamethoxazole per 1 ml of drinking water was given 7 d before and 2 wk after irradiation).

Intracerebral injection

Animals were anesthetized with isoflurane (Baxter Healthcare Corporation) and placed on a stereotaxic apparatus (David Kopf Instruments). The injection site was reached using a small cannula (28 gauge; Plastic One) at the coordinates −2.0 mm lateral and −3.0 mm dorsoventral from the bregma. The animals received an infusion of 1 μl of either sterile saline, 1 μg/μl of recombinant human WT SOD1, or 1 μg/μl of recombinant G93A mutant of human SOD1 protein (provided by M. Urushitani, Shiga University of Medical Science, Shiga, Japan) solution over a period of 2 min by a microinjection pump (A-99; Razel Scientific Instruments). The animals were killed at different time points (3, 24, or 168 h) after the injection.

Tissue collection

Mice were deeply anesthetized via an intraperitoneal injection of a mixture of ketamine hydrochloride and xylazine and rapidly perfused transcardially with 0.9% saline followed by ice-cold borax-buffered 4% PFA, pH 9.5. Brains and spinal cords were rapidly removed from the animals, postfixed for 2–3 d, and placed in a solution containing 10% sucrose diluted in 4% PFA-borax buffer overnight at 4°C. The frozen tissues were mounted on a microtome (Reichert-Jung; Cambridge Instruments Company) and cut into 25-μm coronal sections. The slices were collected in a cold cryoprotectant solution (0.05 M sodium phosphate buffer, pH 7.3, 30% ethylene glycol, and 20% glycerol) and stored at −20°C.

In situ hybridization, immunohistochemistry, and immunofluorescence

In situ hybridization, immunohistochemistry, and immunofluorescence were performed as described previously (Laflamme et al., 1999; Millecamps et al., 2006; Simard et al., 2006). ^{35}S-labeled complementary RNA probes for IL-1β, TLR2, MCP-1, TNF-α, IκBα, IL-12, and mouse PLP1 were used for in situ hybridization. For immunohistochemistry and immunofluorescence, rabbit polyclonal anti-ionized calcium binding adaptor molecule 1 (Iba-1, 1:2,000; Wako Chemicals USA) was used as the primary antibody. Microglia that were immunoreactive for Iba-1 were counted in the lumbar spinal cord using unbiased stereological techniques. The density of labeled cells was estimated by the optical fractionator method using Stereo Investigator software (MBF Bioscience). The lumbar spinal cord was traced with a 10× Plan Apochromat objective and sampled using a 40× Plan Apochromat objective (Nikon). The counting parameters were the distance between counting frames (300 μm), the counting frame size (100 × 100 μm), the dissector height (13 μm), and the guard zone thickness (1.5 μm).

Morphological and morphometric analysis

Mice were deeply anesthetized, perfused with 0.9% saline, and fixed with 3% glutaraldehyde in PBS buffer, pH 7.4. L5 roots and dorsal root ganglion tissue samples were immersed in fixative overnight, rinsed in PBS buffer, and postfixed in 1% osmium tetroxide. After three washes with PBS buffer, samples were dehydrated in a graded series of ethanol and embedded in Epon (Marivac). The thin sections of L5 ventral root were stained with toluidine blue and examined under a light microscope. Axons in the L5 ventral root were counted with Stereo Investigator software.

FJB staining

FJB method was performed as described previously (Turrin and Rivest, 2006). In brief, mounted brain sections were dried under a vacuum, dehydrated through graded concentrations of alcohol (50, 70, and 100% for 1 min), rehydrated through graded concentrations of alcohol (100, 70, and 50% for 1 min), and rinsed for 1 min in distilled water. They were then dipped and shaken in 0.06% potassium permanganate for 10 min, rinsed for 1 min in distilled water, dipped, and shaken in a solution containing 0.004% FJB (Histochem), 0.1% acetic acid, and 0.0002% DAPI (Invitrogen) for 20 min. The slides were thereafter rinsed three times in distilled water for 1 min each, dried, dipped in xylene three times for 2 min each, and coverslipped with distrene plasticizer xylene mounting media (Electron Microscopy Sciences). The number of FJB-positive cells was counted and estimated with Stereo Investigator software.

Nissl staining and motor neuron counting

Mouse lumbar spinal cord was cut into 25-μm-thick transversal sections. The sections were washed in distilled water, dehydrated through graded concentrations of alcohol (50, 70, 95, and 100%) to xylene, rehydrated through graded concentrations of alcohol (100, 95, 70, and 50%), and then stained with a 0.25% thionin solution. Thereafter, the sections were dehydrated and coverslipped. After the staining, the large motor neurons in the ventral horn were counted with Stereo Investigator software. Only large multipolar motor neurons with a cross-sectional area $\geq 250\ \mu m^2$ were considered (Fischer et al., 2004).

Assessment of motor function

The motor function was tested using a rotarod device (10 rpm; Economex Controlier; Columbus Instruments) weekly. The amount of time the mice remained on the rotarod was recorded for up to 180 s. The trial was conducted three times for each mouse and the best result of these trials is used as the riding time of each mouse.

Confocal laser scanning and regular microscopy

For cell phenotyping, tissue samples were analyzed for colocalization with cell type–specific markers using a confocal laser scanning microscope (BX-61) equipped with imaging software (Fluoview SV500 4.3; both from Olympus). Confocal images were acquired with a 60× Plan Apochromat oil-immersion objective (NA 1.35; Olympus) by sequential scanning using a two-frame Kalman filter, low speed scans, and a z separation of 0.40 μm. Regular 2D images were captured on a microscope (C-80; Nikon) fitted to a digital camera (Retiga EXi Fast; QImaging) and a super-high-pressure mercury lamp (Nikon). The images were then processed to enhance contrast and sharpness using Photoshop CS2 and figures were assembled using Illustrator CS (both from Adobe).

Quantitative analysis

Quantitative analyses of hybridization signals were performed as described previously (Glezer et al., 2003). The intensity of mRNA signals were measured on x-ray film (Biomax M_r; Kodak) under a desktop illuminator (Northern Light; GE Healthcare) using a video system (Charge-coupled device video camera module 10.5–15 V; Sony) attached to a 55-mm extension tube set (Vivitar; Micro-Nikkor) for a Nikon lens and coupled to a computer and ImageJ software (1.23p). The OD for each pixel was calculated using a known standard of intensity and distance measurements from a logarithmic specter adapted from BioImage Visage 110s (Millipore).

Statistical analysis

The data were analyzed by one-way analysis of variance followed by Bonferroni's post hoc analysis. $P < 0.05$ was considered statistically significant.

Online supplemental material

Fig. S1 shows distribution of BMDM in WT and $SOD1^{G37R}$ chimeric mice. Table S1 shows recruitment of BMDM (GFP+/Iba-1+) in the CNS of GFP–$SOD1^{G37R}$ mice at 3, 6, and 8 mo after transplantation. Online supplemental material is available at http://www.jcb.org/cgi/content/full/jcb.200705046/DC1.

We thank Dr. M. Urushitani for providing the recombinant human WT and mutant SOD1 proteins, Dr. Mohammed Filali for his technical assistance in motor function test, and Dr. Denis Soulet for helping with the confocal microscope and artwork. MyD88-deficient and SOD1 transgenic breeding pairs were generously obtained from Dr. S. Akira and Dr. J.P. Julien, respectively.

This work was supported by the Canadian Institutes of Health Research (grant RMF 72554). S. Rivest holds a Canadian Research Chair in neuroimmunology.

Submitted: 8 May 2007
Accepted: 15 November 2007

References

Adachi, O., T. Kawai, K. Takeda, M. Matsumoto, H. Tsutsui, M. Sakagami, K. Nakanishi, and S. Akira. 1998. Targeted disruption of the MyD88 gene results in loss of IL-1- and IL-18-mediated function. *Immunity*. 9:143–150.

Akira, S., S. Uematsu, and O. Takeuchi. 2006. Pathogen recognition and innate immunity. *Cell*. 124:783–801.

Beers, D.R., J.S. Henkel, Q. Xiao, W. Zhao, J. Wang, A.A. Yen, L. Siklos, S.R. McKercher, and S.H. Appel. 2006. Wild-type microglia extend survival in PU.1 knockout mice with familial amyotrophic lateral sclerosis. *Proc. Natl. Acad. Sci. USA*. 103:16021–16026.

Boillee, S., K. Yamanaka, C.S. Lobsiger, N.G. Copeland, N.A. Jenkins, G. Kassiotis, G. Kollias, and D.W. Cleveland. 2006. Onset and progression in inherited ALS determined by motor neurons and microglia. *Science*. 312:1389–1392.

Clement, A.M., M.D. Nguyen, E.A. Roberts, M.L. Garcia, S. Boillee, M. Rule, A.P. McMahon, W. Doucette, D. Siwek, R.J. Ferrante, et al. 2003. Wild-type nonneuronal cells extend survival of SOD1 mutant motor neurons in ALS mice. *Science*. 302:113–117.

Corti, S., F. Locatelli, C. Donadoni, M. Guglieri, D. Papadimitriou, S. Strazzer, R. Del Bo, and G.P. Comi. 2004. Wild-type bone marrow cells ameliorate the phenotype of SOD1-G93A ALS mice and contribute to CNS, heart and skeletal muscle tissues. *Brain*. 127:2518–2532.

Fischer, L.R., D.G. Culver, P. Tennant, A.A. Davis, M. Wang, A. Castellano-Sanchez, J. Khan, M.A. Polak, and J.D. Glass. 2004. Amyotrophic lateral sclerosis is a distal axonopathy: evidence in mice and man. *Exp. Neurol.* 185:232–240.

Glezer, I., H. Zekki, C. Scavone, and S. Rivest. 2003. Modulation of the innate immune response by NMDA receptors has neuropathological consequences. *J. Neurosci.* 23:11094–11103.

Gong, Y.H., A.S. Parsadanian, A. Andreeva, W.D. Snider, and J.L. Elliott. 2000. Restricted expression of G86R Cu/Zn superoxide dismutase in astrocytes results in astrocytosis but does not cause motoneuron degeneration. *J. Neurosci.* 20:660–665.

Gowing, G., F. Dequen, G. Soucy, and J.P. Julien. 2006. Absence of tumor necrosis factor-alpha does not affect motor neuron disease caused by superoxide dismutase 1 mutations. *J. Neurosci.* 26:11397–11402.

Gurney, M.E., H. Pu, A.Y. Chiu, M.C. Dal Canto, C.Y. Polchow, D.D. Alexander, J. Caliendo, A. Hentati, Y.W. Kwon, H.X. Deng, et al. 1994. Motor neuron degeneration in mice that express a human Cu,Zn superoxide dismutase mutation. *Science*. 264:1772–1775.

Johnston, J.A., M.J. Dalton, M.E. Gurney, and R.R. Kopito. 2000. Formation of high molecular weight complexes of mutant Cu, Zn-superoxide dismutase in a mouse model for familial amyotrophic lateral sclerosis. *Proc. Natl. Acad. Sci. USA*. 97:12571–12576.

Julien, J.P. 2001. Amyotrophic lateral sclerosis. Unfolding the toxicity of the misfolded. *Cell*. 104:581–591.

Kawai, T., O. Takeuchi, T. Fujita, J. Inoue, P.F. Muhlradt, S. Sato, K. Hoshino, and S. Akira. 2001. Lipopolysaccharide stimulates the MyD88-independent pathway and results in activation of IFN-regulatory factor 3 and the expression of a subset of lipopolysaccharide-inducible genes. *J. Immunol.* 167:5887–5894.

Laflamme, N., S. Lacroix, and S. Rivest. 1999. An essential role of interleukin-1β in mediating NF-κB activity and COX-2 transcription in cells of the blood-brain barrier in response to systemic and localized inflammation, but not during endotoxemia. *J. Neurosci.* 19:10923–10930.

Laflamme, N., G. Soucy, and S. Rivest. 2001. Circulating cell wall components derived from gram-negative and not gram-positive bacteria cause a profound transcriptional activation of the gene encoding Toll-like receptor 2 in the CNS. *J. Neurochem.* 79:648–657.

Millecamps, S., J. Robertson, R. Lariviere, J. Mallet, and J.P. Julien. 2006. Defective axonal transport of neurofilament proteins in neurons overexpressing peripherin. *J. Neurochem.* 98:926–938.

Nguyen, M.D., J.P. Julien, and S. Rivest. 2001. Induction of proinflammatory molecules in mice with amyotrophic lateral sclerosis: no requirement for proapoptotic interleukin-1beta in neurodegeneration. *Ann. Neurol.* 50:630–639.

Nguyen, M.D., J.P. Julien, and S. Rivest. 2002. Innate immunity: the missing link in neuroprotection and neurodegeneration? *Nat. Rev. Neurosci.* 3:216–227.

Nguyen, M.D., T. D'Aigle, G. Gowing, J.P. Julien, and S. Rivest. 2004. Exacerbation of motor neuron disease by chronic stimulation of innate immunity in a mouse model of amyotrophic lateral sclerosis. *J. Neurosci.* 24:1340–1349.

Pramatarova, A., J. Laganiere, J. Roussel, K. Brisebois, and G.A. Rouleau. 2001. Neuron-specific expression of mutant superoxide dismutase 1 in transgenic mice does not lead to motor impairment. *J. Neurosci.* 21:3369–3374.

Rosen, D.R., T. Siddique, D. Patterson, D.A. Figlewicz, P. Sapp, A. Hentati, D. Donaldson, J. Goto, J.P. O'Regan, H.X. Deng, et al. 1993. Mutations in Cu/Zn superoxide dismutase gene are associated with familial amyotrophic lateral sclerosis. *Nature*. 362:59–62.

Rouaux, C., I. Panteleeva, F. René, J.L. Gonzalez de Aguilar, A. Echaniz-Laguna, L. Dupuis, Y. Menger, A.L. Boutillier, and J.P. Loeffler. 2007. Sodium valproate exerts neuroprotective effects in vivo through CREB-binding protein-dependent mechanisms but does not improve survival in an amyotrophic lateral sclerosis mouse model. *J. Neurosci.* 27:5535–5545.

Simard, A.R., and S. Rivest. 2004. Bone marrow stem cells have the ability to populate the entire central nervous system into fully differentiated parenchymal microglia. *FASEB J.* 18:998–1000.

Simard, A.R., D. Soulet, G. Gowing, J.P. Julien, and S. Rivest. 2006. Bone marrow-derived microglia play a critical role in restricting senile plaque formation in Alzheimer's disease. *Neuron*. 49:489–502.

Solomon, J.N., C.A. Lewis, B. Ajami, S.Y. Corbel, F.M. Rossi, and C. Krieger. 2006. Origin and distribution of bone marrow-derived cells in the central nervous system in a mouse model of amyotrophic lateral sclerosis. *Glia*. 53:744–753.

Turner, B.J., J.D. Atkin, M.A. Farg, D.W. Zang, A. Rembach, E.C. Lopes, J.D. Patch, A.F. Hill, and S.S. Cheema. 2005. Impaired extracellular secretion of mutant superoxide dismutase 1 associates with neurotoxicity in familial amyotrophic lateral sclerosis. *J. Neurosci.* 25:108–117.

Turrin, N.P., and S. Rivest. 2006. Tumor necrosis factor alpha but not interleukin 1 beta mediates neuroprotection in response to acute nitric oxide excitotoxicity. *J. Neurosci.* 26:143–151.

Urushitani, M., A. Sik, T. Sakurai, N. Nukina, R. Takahashi, and J.P. Julien. 2006. Chromogranin-mediated secretion of mutant superoxide dismutase proteins linked to amyotrophic lateral sclerosis. *Nat. Neurosci.* 9:108–118.